PCCP

PAPER

View Article Online
View Journal | View Issue

Cite this: *Phys. Chem. Chem. Phys.*, 2016, **18**, 19894

The rich phase behavior of the thermopolarization of water: from a reversal in the polarization, to enhancement near criticality conditions

Irene Iriarte-Carretero,[a] Miguel A. Gonzalez,[a] Jeff Armstrong,[ab] Felix Fernandez-Alonso[bc] and Fernando Bresme*[ad]

Received 7th May 2016,
Accepted 29th June 2016

DOI: 10.1039/c6cp03082c

www.rsc.org/pccp

We investigate using non-equilibrium molecular dynamics simulations the polarization of water induced by thermal gradients using the accurate TIP4P/2005 water model. The full dependence of the polarization covering a wide range of thermodynamic states, from near supercritical to ambient conditions, is reported. Our results show a strong dependence of the thermo-polarization field with the thermodynamic state. The field features a strong enhancement near the critical point, which can be rationalized in terms of the large increase and ultimately the divergence of the thermal expansion of the fluid at the critical temperature. We also show that the TIP4P/2005 model features a reversal in the sign of the thermal polarization at densities $\sim$1 g cm^{-3}. The latter result is consistent with the recent observation of this reversal phenomenon in SPC/E water and points the existence of this general physical phenomenon in water.

1 Introduction

Thermal gradients can induce fascinating non-equilibrium coupling effects in fluids and fluid mixtures. Such effects have been known to exist since the beginning of the 19th century. Ludwig[1] discovered that thermal gradients can induce mass separation. This phenomenon was subsequently investigated by Soret in aqueous solutions.[2] Colloidal suspensions do also exhibit similar behavior, with temperature differences inducing thermophoretic forces that drive the motion of large solutes, *e.g.* polymer particles and biomolecules,[3–6] towards hot (thermophilic) or cold (thermophobic) regions. The specific tendency to drift to hot or cold sources depends very sensitively on the average temperature of the solution, hence opening new avenues to manipulate colloidal suspensions and solutions under bulk and also confinement conditions. Recently, it has been shown that thermal gradients can induce large non-equilibrium concentration fluctuations, which lead to Casimir-like forces in liquid mixtures.[7] In micro and nano devices, these thermal coupling effects may become very relevant.[8–10] Further, in water, thermal gradients can polarize the fluid and generate sizable electrostatic fields.[11] Thermal gradients do also induce molecular orientation in non-polar fluids.[12]

The thermal coupling effects discussed above modify and define the heat transport mechanisms of molecular fluids. Non-equilibrium thermodynamics predicts that the coupling of heat and mass fluxes influences the thermal conductivity of mixtures.[13] de Groot and Mazur suggested in their seminal work[13] that the reduction in the thermal conductivity is expected to be of the order of a few per cent.[13] These coupling effects has been explored systematically and they have been corroborated using equilibrium and non-equilibrium simulations.[14–20] The possibility of a thermal polarization response in water and aqueous solutions provides a new dimension to these studies. Given the pivotal importance of water as solvent in science, engineering and biology, it is important to understand and predict the general dependence of these polarization effects. This should help to advance our understanding of the microscopic mechanisms determining the unusual thermal transport of water and aqueous solutions with temperature and density.

We have recently studied the thermal polarization (TP) of SPC/E water.[21] The strength of the effect was quantified using the thermo-polarization coefficient, $S_{TP} = E/\nabla T$, where E represents the field induced by the thermal gradient, ∇T. A sign change in the TP coefficient at high densities and $\sim$300 K was observed. This sign change defines a reversal in the polarization of water, which is remarkable, as it appears to represent the first such reversal of a non-equilibrium response for a pure fluid. This physical behavior is reminiscent of the one observed in other coupling effects, in particular the Soret effect. The Soret coefficient changes sign at a

[a] *Department of Chemistry, Imperial College London, SW7 2AZ, London, UK. E-mail: f.bresme@imperial.ac.uk*
[b] *ISIS Facility, Rutherford Appleton Laboratory, Chilton, Didcot, Oxfordshire, OX11 0QX, UK*
[c] *Department of Physics and Astronomy, University College London, Gower Street, London, WC1E 6BT, UK*
[d] *Department of Chemistry, Norwegian University of Science and Technology (NTNU), Trondheim, Norway NO-7491*

specific temperature, indicating a reversal in the affinity of solutes (ions, colloids or polymers) to concentrate/move to the hot or cold regions. The dependence of the TP field mirrors the thermal expansion of the fluid,[21] namely, the field becomes stronger when the thermal expansion increases. This physical principle may suggest new approaches to maximize the TP electrostatic field. Indeed near criticality the thermal expansion increases dramatically, ultimately diverging at the critical point. It has been shown that thermophoretic transport, *e.g.* the Soret coefficient, diverges as the critical point is approached. In general, transport coefficients behave anomalously in the critical region.[22,23] Hence, we want to investigate whether a similar enhancement behavior can be observed in the TP effect. We address this question in the present work.

We have chosen for our study the TIP4P/2005 model,[24] as it is widely regarded as the most accurate rigid non-polarizable model of water. One of the key ingredients of the success of this water model is the good reproduction of the ratio of the dipole and quadrupole moments of the water molecule.[25] The TIP4P/2005 model predicts accurately the thermophysical properties of water in a wide range of thermodynamic conditions. It also provides a good account of the critical temperature and critical density of water,[26] and a good representation of the ice-water phase diagram.[27] The TIP4P/2005 model has also been used to study the properties of supercooled water,[28–30] to interpret the anomalous behavior of water[31] and to compute the thermal conductivity of water.[32,33] This model reproduces the anomalous increase of the thermal conductivity with temperature, which is characteristic of water. Given the accuracy and general interest of the TIP4P/2005 model in the investigation of water and aqueous solutions, it represents a good starting point to analyze the general dependence of the TP effect. Our results should therefore provide a benchmark and new challenges for future experimental studies of the TP effect and thermal transport of water.

Our paper is structured as follows. In Section 2 we discuss the computational details of the non-equilibrium molecular dynamics simulations and models employed in this work. A discussion of the thermal polarization of water with reference to the phase diagram of TIP4P/2005 water follows. Our conclusions and final remarks close the paper.

2 Methodology

The simulations were performed using the non-equilibrium molecular dynamics (NEMD) method, following the approach discussed in ref. 32. The thermal gradient is imposed using previously introduced boundary conditions,[18,34] which enable the set up of the thermal gradient preserving the periodicity of the simulation cell. In the typical implementation of the NEMD method the simulation is performed using a prismatic simulation box, elongated in the z direction, *i.e.* $L_z > L_x = L_y$. Thermostatting layers, with a typical thickness of 0.09–0.16 nm, were defined at the edges and the middle of the simulation box. The oxygen atoms in the water molecules initially located in the hot and cold thermostats were restrained in the direction of the heat flux, z, using a harmonic restraining potential with a force constant of 1000 kJ mol^{-1} nm^{-2}. The molecules were left free to rotate and also translate in the directions x and y perpendicular to the flux vector. These molecules were thermostatted every timestep using the velocity rescale algorithm.[35] In our method, unrestrained molecules can enter and leave the thermostatting regions freely, and they are not thermostatted directly, but can exchange momentum with the restrained molecules, hence becoming hotter or colder.

The simulations were performed in a prismatic box with dimensions $\{L_x,L_y,L_z\}/L_x = \{1,1,10\}$ with L_x = 2.54 nm. The number of unrestrained water molecules was varied between, 2224 and 5344, to achieve different average densities and to investigate different pressure conditions. The number of restrained molecules in the thermostatting layers was set to 38, both at the hot and cold thermostats. The trajectory was generated by integrating the equations of motion with the leap-frog algorithm with a time step of 2 fs. A typical non-equilibrium simulation for a specific average density and temperature involved 50 ns. 10^6 configurations were employed to compute temperature, density and electrostatic field profiles. All the profiles were computed by dividing the simulation box in 300 slabs along the z direction. As discussed below in the results section, we performed additional running averages over these profiles to represent some properties.

The simulations were performed with the TIP4P/2005 model using the parameters reported in ref. 24. The Lennard-Jones potential was truncated and shifted at 1 nm. The smooth particle mesh Ewald summation method[36] was used in order to compute the electrostatic interactions. We have shown in our previous work that this approach predicts polarization fields under thermal gradients in good agreement with those obtained from an exact treatment of the Coulombic interactions. All the computations were performed with the code GROMACS v 4.5.5.[37]

The electrostatic field in the direction of the heat flux was computed from the integral of the charge density,

$$E(z) = \frac{1}{\varepsilon_0}\int_0^z \rho_q(z')\mathrm{d}z' \qquad (1)$$

where ε_0 is the permittivity of vacuum, $\rho_q(z) = \sum_{i=1}^{N}\delta(z-z_i)q_i \Big/ A$ is the charge density at z, and $A = L_x \times L_y$ is the simulation box cross sectional area. The sum in eqn (1) runs over all the charges, q_i, in the simulation box. For the TIP4P/2005 model these are defined by the charge of the hydrogen, q_H = 0.5564 e and the charge $q_M = -2q_H$ of the virtual site. The lower limit in the eqn (1) is given by the box origin, which is set to "0".

The charge density was also obtained from an expansion in dipolar and quadrupolar terms.[21,38–41] The projection of these contributions along the heat flux direction, z is given by,

$$\rho_{q,m}(z) = -\frac{\mathrm{d}}{\mathrm{d}z}\left(P_z(z) - \frac{\mathrm{d}Q_{zz}(z)}{\mathrm{d}z}\right) \qquad (2)$$

Although higher order terms can be included to calculate the charge density, these two terms provide an accurate representation of the field obtained *via* eqn (1) (see discussion in the

results section below). The dipolar and quadrupolar contributions were computed using the equations,[38,39]

$$P_z(z) = \frac{1}{A}\left\langle \sum_{i=1}^{N_m} \delta(z - z_i)\left[\sum_{j=1}^{j\in m} q_{j,m} z_{j,m}\right]\right\rangle \quad (3)$$

$$Q_{zz}(z) = \frac{1}{A}\left\langle \sum_{i=1}^{N_m} \delta(z - z_i)\left[\frac{1}{2}\sum_{j=1}^{j\in m} q_{j,m} z_{j,m}^2\right]\right\rangle \quad (4)$$

where the index i in the first sum runs over the number of molecules, N_m, and the index j in the second sum runs over the number of charged sites in the molecule, with $z_{j,m}$ representing the z-coordinate of the charged site, j (hydrogen or virtual site) in molecule m relative to the position of the molecule. For the latter we used the coordinates of the virtual site in the TIP4P/2005 model. The dipolar and quadrupolar contributions define the molecular electrostatic field.

$$\begin{aligned} E_{\mathrm{mol}}(z) &= E_{\mathrm{P}}(z) + E_{Q_{zz}}(z) \\ &= \frac{-1}{\varepsilon_0}\int_0^z \frac{\mathrm{d}P_z(z')}{\mathrm{d}z'}\mathrm{d}z' + \frac{1}{\varepsilon_0}\int_0^z \frac{\mathrm{d}^2 Q_{zz}(z')}{\mathrm{d}z'^2}\mathrm{d}z', \end{aligned} \quad (5)$$

Eqn (1) and (5) can be used to compute the field induced by the thermal gradients. The strength of this field varies linearly with the thermal gradient according to the non-equilibrium thermodynamics phenomenological equation,[11]

$$E = \left(1 - \frac{1}{\varepsilon_{\mathrm{r}}}\right)\frac{L_{pq}}{L_{pp}}\frac{\nabla T}{T}, \quad (6)$$

where the ratio of the phenomenological coefficients, L_{pq}/L_{pp}, the fluid relative permittivity, ε_{r}, thermal gradient ∇T and the temperature T, determine the strength of the thermal polarization field. As usual in the context of the non-equilibrium thermodynamics the cross coefficient, L_{pq} in this case, quantifies the coupling effect, and it can be positive, negative or zero. To quantify the thermal polarization induced by the thermal gradient we use the thermopolarization coefficient $S_{\mathrm{TP}} = E/\nabla T$.

3 Results

The NEMD algorithm discussed above produces stable trajectories over long simulation times, $\sim$50 ns, as indicated by a stable potential energy (see Fig. 1), as well as stable kinetic and total energies (not shown). Fig. 1 shows representative temperature profiles for the unrestrained molecules, where deviations from linearity indicate variations in the thermal conductivity along the simulation box. We exploited this fact in our previous work to compute the thermal conductivity of water using a single NEMD simulation.[32] The temperature profile also induces a density profile, as a result of the thermal expansion of the fluid. The pairs of density and temperature generated by the NEMD method can be used to calculate the equation of state of TIP4P/2005 water.[32] All the results presented below were obtained by discarding the layers in the neighborhood of the thermostatting regions, typically 14–18 slabs. The symmetry of the thermal gradients was exploited in order to average the results on both sides of the box in order to reduce the statistical uncertainty of our results. Our NEMD simulations (see Fig. 1) involve large thermal gradients of $\sim 10^{10}$ K m^{-1}. As discussed before, even for such large gradients the fluid features a linear response (see *e.g.* ref. 11 and 42).

We show in Fig. 2 the behavior of the thermo-polarization field for a representative thermodynamic state. The break in symmetry induced by the thermostats results in large variations in the charge density and large local fields. These fields disappear quickly as we move into the "bulk" region between the two thermostats. As expected, the field in this region is defined by the unrestrained molecules. The magnitude of the field obtained here for the TIP4P/2005 model, 10^7 V m^{-1} for $\nabla T \sim 10^{10}$ K m^{-1} is of the same order as the one reported before for the SPC/E water model using a different NEMD implementation and a different simulation code.[21,41,42] The TP field features a strong variation along the simulation box, increasing by a factor of 4 between 2 and 10 nm (see arrows in Fig. 2-middle). It has been found recently that the TP field of the SPC/E model is proportional to the thermal expansion of the liquid.[21] To test this idea in the TIP4P/2005 model, we computed the thermal expansion for the system investigated in Fig. 2. Firstly, we constructed the equation of state by using the pairs of density and temperature in the simulation box, and the thermal expansion, $\alpha = -1/\rho(\partial\rho/\partial T)_{\mathrm{p}}$, was obtained by calculating the numerical derivative. The induced field correlates well with the variation of the thermal expansion with temperature (or as we move from the cold region – 2 nm to the

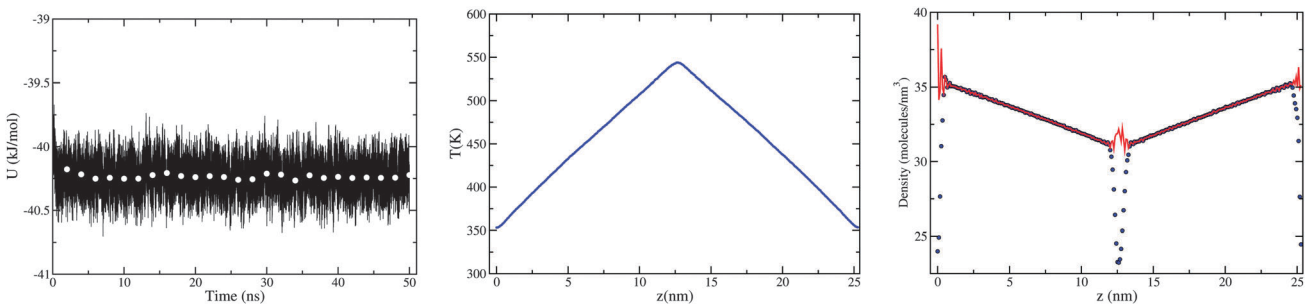

Fig. 1 (left) Instantaneous (black line) potential energy for a representative non-equilibrium run. The white circles represent sub averages over 2 ns. (middle) Temperature profile of the unrestrained water molecules. (right) Density profile of the unrestrained water molecules (circles) and all the molecules (red line). All the data were obtained using a non-equilibrium simulation with average temperature 451 ± 0.1 K.

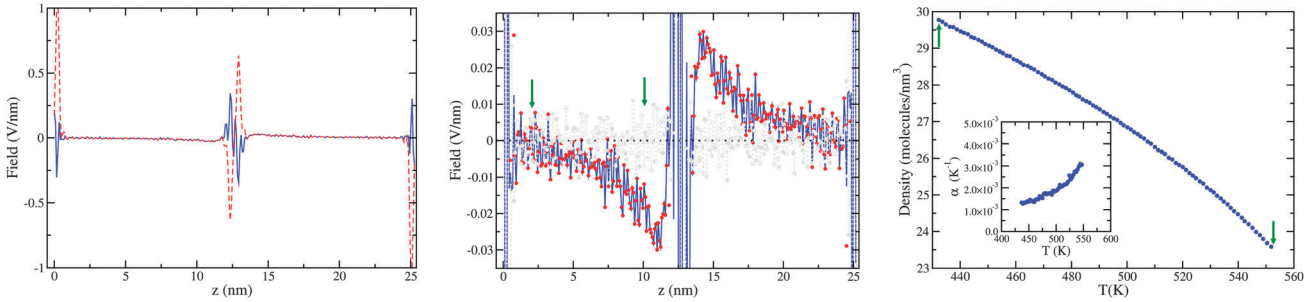

Fig. 2 (left) Total electrostatic field (blue line) and field associated to the unrestrained water molecules (red line). (middle) Zoom into the thermal polarization field generated between the hot and cold thermostats. The blue line represents the total field and the red circles the field associated to the unrestrained water molecules. The grey line and circles represent the field for a system without a thermal gradient, corresponding to a thermodynamic state at constant temperature, 500 K, and constant density, 26.7 molecules per nm^3 (0.798 g cm^{-3}). (right) Equation of state obtained from NEMD simulations. The green arrows indicate the interval used to analyze the equation of state. The inset represents the thermal expansion coefficient obtained from the numerical derivative of the equation of state, $\alpha = -1/\rho(\partial\rho/\partial T)_p$. A running average over 7 points was applied to the equation of state to smooth out the data before calculating the derivative. All the data were obtained for a non-equilibrium simulation with average temperature of 492 ± 0.2 K. All the data were obtained by averaging the left and right data in the simulations, hence exploiting the symmetry of the thermal gradient around the center of the box. The electrostatic fields were computed from direct integration of the charge density using eqn (1).

hot region – 10 nm), and becomes stronger as the thermal expansion of the liquid increases.

As a consistency check we have performed additional simulations without a thermal gradient, with a uniform temperature of 500 K. In these simulations we maintained the same set up used for the NEMD simulations, namely the restrained molecules in the hot and cold layers, but all the molecules where thermostatted using the v-rescale thermostat. These simulations (see Fig. 2) show the absence of an electrostatic field in the bulk region, as one would expect in the absence of the non-equilibrium coupling effect. This computation also serves as a test of our approach of restraining water molecules in the thermostatting layers, to make sure this does not lead to residual electrostatic fields.

We discussed in the methodology section two approaches to compute the thermo-polarization field. The equivalence of the fields obtained from eqn (1) – atomistic – and eqn (5) – molecular – is analyzed in Fig. 3. The agreement between the two methods is excellent, showing that the dipolar and quadrupolar components account well for the full electrostatic field. For the thermodynamic state represented in Fig. 3, dipolar and quadrupolar terms contribute with opposite sign to the total field, with the quadrupolar term being dominant. This behavior is reminiscent of that found previously in systems involving inhomogeneities in the density, namely the liquid-vapor interface,[38–40] using other water models, a behavior that can be traced back to the large quadrupole of the water molecule. Interestingly, our TP field features a minimum. Advancing the discussion below, we discern that the minimum is connected to the vicinity of this thermodynamic state to the critical region and the larger thermal expansion coefficient of water in that region.

Following the analyses of the systems presented above, we have performed an investigation of the thermal polarization of water considering a wide range of thermodynamic states (see Fig. 4). The thermodynamic states target average densities at near critical conditions and at high densities characteristic of liquid states. Along with the non-equilibrium simulation

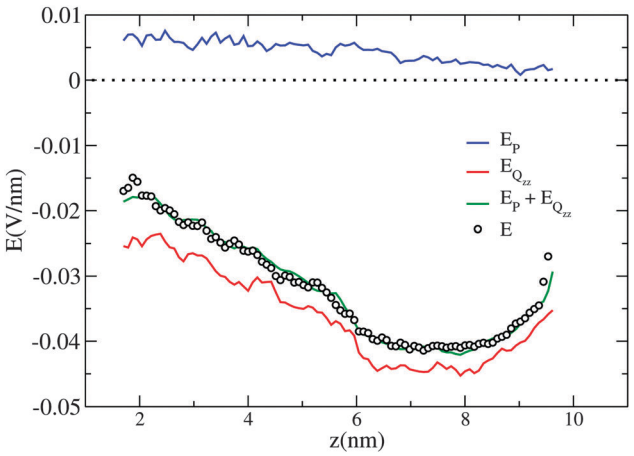

Fig. 3 Electrostatic field obtained from eqn (1) and (5). The fields have been represented applying a running average over 10 points. The simulation corresponds to an average temperature of 676 ± 0.3 K.

data we have represented the equation of state for a thermodynamic state close to the critical point. The agreement between the NEMD and *NpT* data is excellent, hence verifying the local equilibrium hypothesis. The thermodynamic states investigated here vary in the temperature range, 250 K, at high densities, to ~900 K at near critical densities. In is way we cover a wide range of states featuring significant variation in the thermal expansion coefficient (see slope of the curves, dρ/dT in Fig. 4). Following the connection between the TP field and the thermal expansion mentioned earlier we expect significant changes in the TP coefficient, S_{TP}, as we move through the temperature/density plane. Data for the binodal line obtained in this work and results from ref. 43 are also reported in Fig. 4. The deviations between the two sets of data are small despite the different cutoffs employed in the computations. Hence, we expect that the critical point for our cutoff will be close to the one estimated in ref. 43.

We show in Fig. 5 the dependence of S_{TP} for a selection of systems investigated in this work, targeting high, intermediate

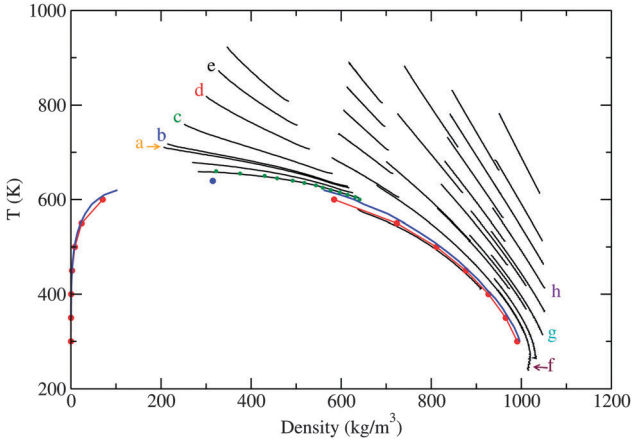

Fig. 4 Isobars of all the systems investigated in this work (full black lines). (Red points/line) Binodal lines of the TIP4P/2005 model obtained in this work, from the analysis of *NVT* equilibrium simulations using an explicit water slab. (Blue lines and blue circle) coexistence line and critical point reported in ref. 43 using a cutoff of 0.8 nm and long range corrections for the pressure. The letters indicate isotherms that are analyzed in Fig. 5. The dots represent results from *NpT* equilibrium simulations at 220 bar.

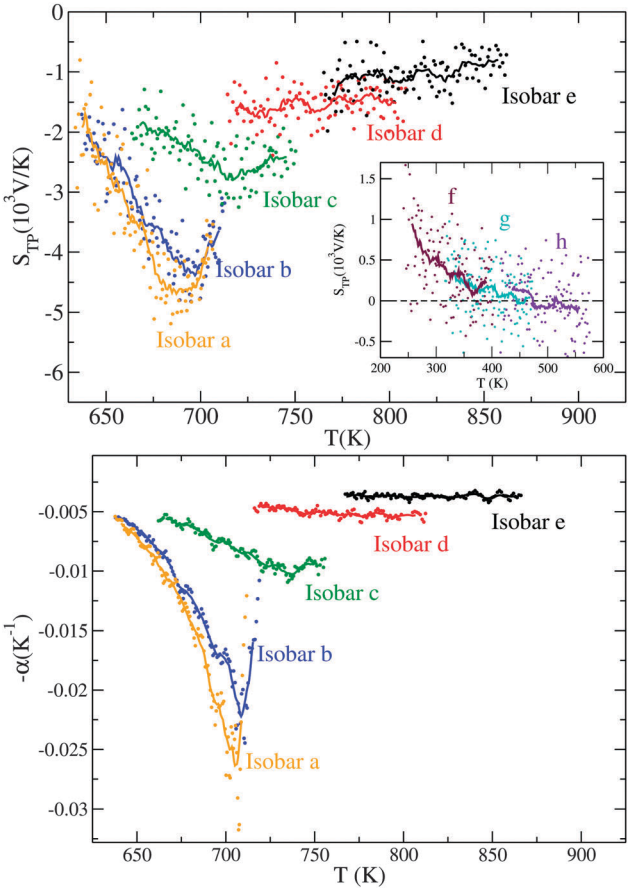

Fig. 5 (top) Dependence of the thermopolarization coefficient, $S_{TP} = E/\nabla T$ with temperature for different isobars. The inset shows the change in the sign of the TP field as the temperature decreases. (bottom) Negative of the thermal expansion coefficient for the systems investigated in the top figure. The letters refer to the isobars represented in Fig. 4.

and low densities. These systems summarize the main physics of the TP effect. At high densities, characteristic of the liquid phase and temperatures near 300–400 K the TP coefficient is positive (see inset in Fig. 5), of the order of 10^{-4} V K^{-1}. At higher temperatures the TP coefficient changes sign and becomes negative. At higher temperatures and lower densities the TP coefficient increases drastically, particularly when the system approaches the critical point conditions, where the coefficient reaches values of $\sim 10^{-3}$–10^{-2} V K^{-1}, *i.e.*, one/two orders of magnitude larger than the response at near ambient temperatures ($T \sim 300$ K). The dependence of the TP coefficient with temperature and density shows an overwhelming correlation with the temperature/density dependence of the thermal expansion (see Fig. 5). This is particularly evident for the systems near the critical point, where the TP coefficient features a clear enhancement (a minimum, *i.e.* maximum strength in absolute value) at the temperature where the thermal expansion coefficient reaches a maximum (see Fig. 5).

Fig. 6 summarizes all the results obtained in this work. This plot shows the global dependence of the thermal polarization field of water on the T/ρ plane for our studied states. The phase coexistence diagram of TIP4P/2005 water is shown to provide a reference of the thermodynamic state. The regions where the TP field features a sign inversion have been highlighted. We found that this region is quite wide, since the field features a slow variation with temperature (see inset in Fig. 5-top). Fig. 6 shows a similar graph for the quadrupolar contribution. These data demonstrate that the quadrupolar term features a strong dependence with temperature and density mirroring the change in the thermal expansion coefficient. Following the dependence of the thermal expansion near the critical region, the quadrupolar term does also feature an enhancement in that region. Overall, these results confirm the idea that the quadrupolar contribution is chiefly responsible for the magnitude of the TP field, and the combination of dipolar and quadrupolar contributions plays a key role in determining the region of temperature/density where the reversal of the polarization is observed.

The TP coefficient features a significant enhancement near the critical region (see Fig. 6). The enhancement can be better seen in Fig. 7 where we represent the coefficient for different isochores, as a function of the distance from the critical point of TIP4P/2005. Our results distinctly show a strong enhancement in the thermal polarization as the critical point is approached. For the closest temperature to the critical point investigated here, the TP coefficient increases by two orders of magnitude as compared with the values obtained at $T \sim 300$ K. It has been discussed before in the context of binary mixtures, that the Soret coefficient diverges at the critical point.[23] Experiments of aniline–cyclohexane mixtures[44] agree with the predictions from theoretical arguments, and good agreement is obtained with the asymptotic power law and the corresponding exponent. We have analyzed the dependence of our TP coefficient with $1 - T_c/T$, which is the reduced temperature normally used to investigate critical behavior. The corresponding results are shown in the inset in Fig. 7 for the 0.31 g cm^{-3} isochore, which corresponds to the critical density of the TIP4P/2005 model.[43]

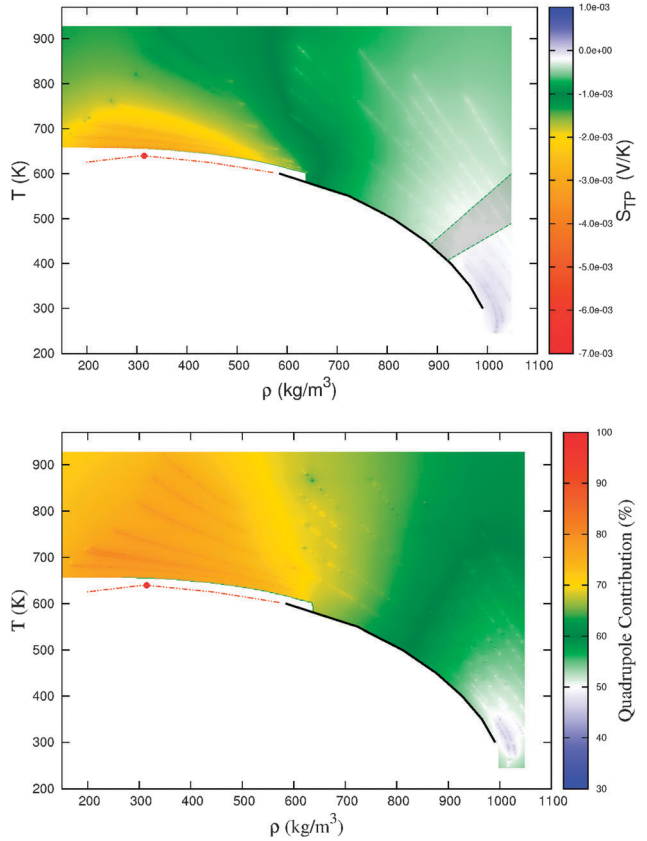

Fig. 6 (top) The thermopolarization coefficient for all the system investigated in this work. The color map indicates the magnitude of the coefficient. The black line represents the liquid branch of the TIP4P/2005 model simulated in this work with a cutoff of 1 nm. The red dashed line represents the coexistence line reported in ref. 43. The grey region represents the area where the TP field reverses sign. (bottom) Quadrupolar contribution to the total TP field expressed as a percentage of the total field.

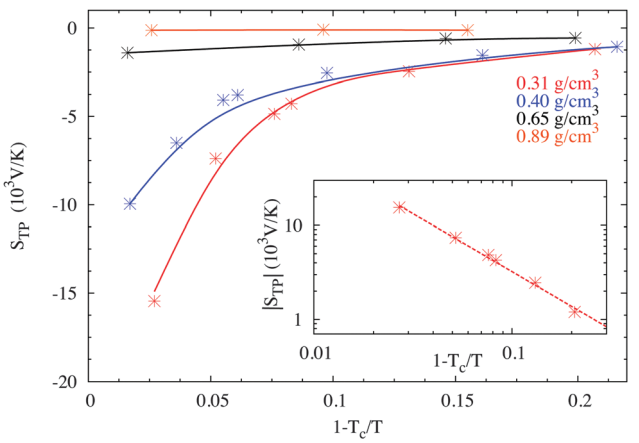

Fig. 7 Dependence of the TP coefficient for different isochores as a function of the reduced temperature, $(1 - T_c/T)$, where T_c = 640 K.[43] The inset shows the dependence of the absolute value of the TP coefficient, $|S_{TP}|$ with $(1 - T_c/T)$ for the 0.31 g cm^{-3} critical isochore, and the dashed line represents the regression line, $0.19(1 - T_c/T)^{-1.239}$ using the 3D Ising critical exponent, 1.239.

The absolute value of the TP coefficient follows the functional dependence, $|S_{TP}| = (1 - T_c/T)^{-\gamma}$. The isothermal compressibility and the thermal expansion diverge along the critical isochore according to $\approx(1 - T_c/T)^{-\gamma'}$, where γ' is the critical exponent. Water belongs to the universality class of Ising-like systems, hence, $\gamma' = 1.239$ for the 3D Ising model.[45] Interestingly, our data can be very well fitted assuming $\gamma = 1.239$ (see Fig. 7). Equation $(1 - T_c/T)^{-\gamma}$ can be used to estimate the thermal polarization closer to the critical point, $(1 - T_c/T) \sim 0.01$, assuming the same power law is fulfilled. In this case, $|S_{TP}|$ could increase by two orders of magnitude.

4 Conclusions and final remarks

Using non-equilibrium molecular dynamics simulations in combination with one of the most accurate empirical rigid force-fields of water, the TIP4P/2005 model, we have investigated the general behavior of the thermal polarization (TP) of water. Our results point towards a strong dependence of the TP coefficient with the thermodynamic state. The magnitude of the TP coefficient is strongly correlated with the variation of the thermal expansion of water with temperature and density. At near critical conditions we found a large enhancement of the TP coefficient, which varies in the interval $+10^{-4}$ V K^{-1}, at near ambient temperatures to -10^{-2} V K^{-1} at near critical conditions. For gradients achievable with *e.g.* optical tweezers and microfluidic chambers 10^{5-6} K m^{-1},[46,47] fields of the order of 10^{1-2} V m^{-1} could be generated at near ambient conditions while these fields could be higher, *e.g.* 10^{2-4} V m^{-1} for the stronger thermal gradients, $\sim 10^{6-8}$ K m^{-1}, that can be generated using metallic particles and other plasmonic structures.[48–50]

The results presented in our work using the TIP4P/2005 model are consistent with the existence of a temperature inversion in the thermal polarization coefficient of SPC/E water. Hence, our results support the generality of this reversal phenomenon in realistic atomistic models of water. This prediction awaits experimental verification. We expect some variability in the exact inversion temperature for different water forcefields, since different models differ in their performance in predicting thermophysical properties.

The large increase of the TP coefficient near the critical point may open a route to perform experimental studies leading to the experimental observation of the TP effect. For a start, for the typical thermal gradients discussed above the resulting TP field could increase significantly, $\sim 10^{3-6}$ V m^{-1} for 10^{5-6} K m^{-1}. Considering that many thermodynamic properties, as well as thermal transport coefficients (Soret coefficient) increase in the critical region and ultimately diverge at the critical point, the study of TP fields at near critical conditions may open new avenues in the investigation of critical phenomena and the behavior of molecular fluids under thermal gradients. The S_{TP}, at the critical density, increases as one approaches the critical point according to, $|S_{TP}| = (1 - T_c/T)^{-\gamma}$, with the exponent, $\gamma = 1.239$, hence following the same power law that governs the divergence of the isothermal compressibility and the thermal

expansion coefficient of water along the critical isochore. This strong dependence with temperature indicates that S_{TP} could substantially increase as one approaches the critical point. The possibility of a divergence, as observed in the thermal expansion, opens an interesting question too. Establishing whether S_{TP} diverges and whether the exponent is the same as reported in our work requires additional investigations. The theory of critical phenomena may provide an approach to find scaling relations for the TP effect. Prospect for future experiments may include the investigation of transient heat fluxes over timescales commensurate with thermalisation or the attainment of a well-defined temperature for all degrees of freedom of the system. For thermal gradients involving 10^{-3}–10^{-1} K nm^{-1}, typical length scales of 100 nm and the diffusion coefficient of water $\sim$0.1 Å^2 ps^{-1}, thermalisation would take place over timescales of $\sim$10 μs. Transient experiments targeting these conditions should operate below this timescale.

Acknowledgements

We thank the EPSRC-UK (EP/J003859/1) and NFR (Project No. 221675) for financial support. The UK Science and Technology Facilities Council is gratefully acknowledged for financial support under Contract No. 3624. We acknowledge the Imperial College High Performance Computing Service for providing computational resources. FB would like to thank the EPSRC for support *via* the award of a Leadership Fellowship.

References

1 C. Ludwig, *Sitzungsber. Akad. Wiss. Wien, Math.-Naturwiss. Kl., Abt. 1*, 1856, **20**, 539.
2 C. Soret, *Arch. Sci. Phys. Nat.*, 1879, **2**, 48.
3 S. Wiegand, *J. Phys.: Condens. Matter*, 2004, **16**, R357.
4 R. Piazza and A. Parola, *J. Phys.: Condens. Matter*, 2008, **20**, 153102.
5 S. Putnam, D. Cahill and G. Wong, *Langmuir*, 2007, **23**, 9221.
6 M. Reichl, M. Herzog, A. Götz and D. Braun, *Phys. Rev. Lett.*, 2014, **112**, 198101.
7 T. Kirpatrick, J. O. de Zarate and J. Sengers, *Phys. Rev. Lett.*, 2015, **115**, 035901.
8 M. Yang and M. Ripoll, *Soft Matter*, 2014, **10**, 1006.
9 A. Lervik and F. Bresme, *Phys. Chem. Chem. Phys.*, 2014, **16**, 13279–13286.
10 Y. He, M. Tsutsui, R. Scheicher, F. Bai, M. Taniguchi and T. Kawai, *ACS Nano*, 2013, **7**, 538.
11 F. Bresme, A. Lervik, D. Bedeaux and S. Kjelstrup, *Phys. Rev. Lett.*, 2008, **101**, 020602.
12 F. Römer, F. Bresme, J. Muscatello, D. Bedeaux and J. Rubi, *Phys. Rev. Lett.*, 2012, **108**, 105901.
13 S. de Groot and P. Mazur, *Non-equilibrium thermodynamics*, Dover, New York, 1984.
14 D. MacGowan and D. Evans, *Phys. Rev. A: At., Mol., Opt. Phys.*, 1986, **34**, 2133.
15 G. Paolini and G. Ciccotti, *Phys. Rev. A: At., Mol., Opt. Phys.*, 1987, **35**, 5156.
16 R. Vogelsang and C. Hoheisel, *Phys. Rev. B: Condens. Matter Mater. Phys.*, 1987, **35**, 3487–3491.
17 R. Vogelsang, C. Hoheisel, G. Paolini and G. Ciccotti, *Phys. Rev. A: At., Mol., Opt. Phys.*, 1987, **36**, 3964.
18 B. Hafskjold, T. Ikeshoji and S. Ratkje, *Mol. Phys.*, 1993, **80**, 1389.
19 N. Miller, P. Daivis, I. Snook and B. Todd, *J. Chem. Phys.*, 2013, **139**, 144504.
20 J. Armstrong and F. Bresme, *Phys. Chem. Chem. Phys.*, 2014, **16**, 12307.
21 J. Armstrong and F. Bresme, *Phys. Rev. E: Stat., Nonlinear, Soft Matter Phys.*, 2015, **92**, 060103.
22 J. Sengers, in *Supercritical Fluids: Fundamentals for Application*, ed. E. Kiran and J. Levelt-Sengers, Kluwer Academic, Dordrecht, 1994, ch. Effects of critical fluctuations on the thermodynamic and transport properties of supercritical fluids, pp. 231–271.
23 J. Luettmer-Strathmann, in *Thermal Nonequilibrium Phenomena in Fluid Mixtures*, ed. W. Köhler and S. Wiegand, Springer Berlin Heidelberg, Berlin, Heidelberg, 2002, ch. Thermodiffusion in the Critical Region, pp. 24–37.
24 J. Abascal and C. Vega, *J. Chem. Phys.*, 2005, **123**, 234505.
25 J. L. F. Abascal and C. Vega, *Phys. Rev. Lett.*, 2007, **98**, 237801.
26 C. Vega and J. Abascal, *Phys. Chem. Chem. Phys.*, 2011, **13**, 19663.
27 J. Abascal, E. Sanz and C. Vega, *Phys. Chem. Chem. Phys.*, 2009, **11**, 556.
28 J. Abascal and C. Vega, *J. Chem. Phys.*, 2010, **133**, 234502.
29 S. Overduin and G. Patey, *J. Chem. Phys.*, 2013, **138**, 184502.
30 F. Bresme, J. Biddle, J. Sengers and M. Anisimov, *J. Chem. Phys.*, 2014, **140**, 161104.
31 A. Nilsson and L. G. M. Pettersson, *Nat. Commun.*, 2015, **6**, 1.
32 F. Römer, A. Lervik and F. Bresme, *J. Chem. Phys.*, 2012, **137**, 074503.
33 T. Sirk, S. Moore and E. Brown, *J. Chem. Phys.*, 2013, **138**, 064505.
34 A. Tenenbaum, *Phys. Rev. A: At., Mol., Opt. Phys.*, 1983, **28**, 3132.
35 G. Bussi, D. Donadio and M. Parrinello, *J. Chem. Phys.*, 2007, **126**, 014101.
36 U. Essmann, L. Perera, M. Berkowitz, T. Darden, H. Lee and L. Pedersen, *J. Chem. Phys.*, 1995, **103**, 8577.
37 B. Hess, C. Kutzner, D. van der Spoel and E. Lindahl, *J. Chem. Theory Comput.*, 2008, **4**, 435.
38 M. Wilson, A. Pohorille and L. Pratt, *J. Chem. Phys.*, 1989, **90**, 5211.
39 J. Glosli and M. Philpott, *Electrochim. Acta*, 1996, **41**, 2145.
40 V. Sokhan and D. Tildesley, *Mol. Phys.*, 1997, **92**, 625.
41 P. Wirnsberger, D. Fijan, A. Saric, M. Neumann, C. Dellago and D. Frenkel, http://arxiv.org/abs/1602.02734, 2016.
42 J. A. Armstrong, C. Daub and F. Bresme, *J. Chem. Phys.*, 2015, **143**, 036101.

43 C. Vega, J. Abascal and I. Nezbeda, *J. Chem. Phys.*, 2006, **125**, 034503.
44 N. Giglio and A. Vendramini, *Phys. Rev. Lett.*, 1975, **34**, 561.
45 J. Sengers and J. L. Sengers, *Annu. Rev. Phys. Chem.*, 1986, **37**, 189.
46 H.-R. Jiang, H. Wada, N. Yoshinaga and M. Sano, *Phys. Rev. Lett.*, 2009, **102**, 208301.
47 S. Duhr and D. Braun, *Phys. Rev. Lett.*, 2006, **96**, 168301.
48 A. O. Govorov, W. Zhang, T. Skeini, H. Richardson, J. Lee and N. A. Kotov, *Nanoscale Res. Lett.*, 2006, **1**, 84–90.
49 J. E. Reiner, J. W. F. Robertson, D. L. Burden, L. K. Burden, A. Balijepalli and J. J. Kasianowicz, *J. Am. Chem. Soc.*, 2013, **135**, 3087–3094.
50 C. R. Crick, P. Albella, B. Ng, A. P. Ivanov, T. Roschuk, M. P. Cecchini, F. Bresme, S. A. Maier and J. B. Edel, *Nano Lett.*, 2015, **15**, 553–559.